Preparation and Characterization of Epoxy/Polyhedral Oligomeric Silsesquioxane Hybrid Nanocomposites

JIEH-MING HUANG,[1] HUI-JU HUANG,[1] YU-XIANG WANG,[1] WEN-YI CHEN,[2] FENG-CHIH CHANG[2]

[1]Department of Chemical and Materials Engineering, Vanung University, 1, Van Nung Road, Chung-Li, 32054, Taiwan, Republic of China

[2]Institute of Applied Chemistry, National Chiao-Tung University, Hsin-Chu, Taiwan, Republic of China

Received 24 October 2008; revised 25 June 2009; accepted 29 June 2009
DOI: 10.1002/polb.21788
Published online in Wiley InterScience (www.interscience.wiley.com).

ABSTRACT: We have prepared epoxy/polyhedral oligomeric silsesquioxane (POSS) nanocomposites by photopolymerization from octakis(glycidylsiloxy)octasilsesquioxane (OG) and diglycidyl ether of bisphenol A. We used nuclear magnetic resonance, Raman, and Fourier transform infrared spectroscopies to characterize the chemical structure of the synthetic OG. Differential scanning calorimetry and dynamic mechanical analysis (DMA) revealed that the nanocomposites possessed higher glass transition temperatures than that of the pristine epoxy resin. Furthermore, DMA indicated that all of the nanocomposites exhibited enhanced storage moduli in the rubbery state, a phenomenon that we ascribe to both the nano-reinforcement effect of the POSS cages and the additional degree of crosslinking that resulted from the reactions between the epoxy and OG units. Thermogravimetric analysis revealed that the thermal stability of the nanocomposites was better than that of the pristine epoxy. © 2009 Wiley Periodicals, Inc. J Polym Sci Part B: Polym Phys 47: 1927–1934, 2009
Keywords: epoxy; nanocomposites; photopolymerization; POSS; thermal properties

INTRODUCTION

Hybrid materials possessing both inorganic and organic components are interesting substances because of their potentially increased performance capabilities relative to those of either of their nonhybrid species. Recently, novel classes of organic/inorganic hybrid materials have been developed based on polyhedral oligomeric silsesquioxane (POSS),[1–7] a cubic form of silica that is rigid, has defined dimensions (0.53 nm), and presents eight organic groups (functional or inert) at the vertices of the cube. POSS derivatives have several advantages over conventional inorganic fillers, including monodispersity, low density, high thermal stability, and controllable functionalities. In addition, POSS monomers can be blended directly with polymers or copolymerized with other monomers to form polymer/POSS nanocomposites. Dispersing an inorganic POSS component uniformly within an organic polymer matrix at the nanoscale level can have a synergistic effect on improving the bulk properties.[8–10] Several nanocomposite hybrid polymers incorporating POSS exhibit increased values of their glass transition (T_g), and decomposition (T_{dec}) temperatures, improved resistance to oxidation, and reduced flammability.[11–13] Incorporating monofunctional or multifunctional POSS-epoxy into the backbone of epoxy resin improves its thermal properties.[14–18] Octakis(glycidyldimethylsiloxy)octasilsesquioxane (OG) is the most-studied epoxy-

Correspondence to: J.-M. Huang (E-mail: jiehming@mail.vnu.edu.tw)

Journal of Polymer Science: Part B: Polymer Physics, Vol. 47, 1927–1934 (2009)

POSS monomer. In addition to its use as a multifunctional monomer, OG is also a reactive additive for the modification of epoxy resins. Laine's group published a series of papers relating to the preparation of epoxy-POSS monomers and their polymers.[19–23] The use of octahedral silsesquioxane (cube) organic/inorganic nanocomposites as model systems for determining nanostructure-processing property relationships to demonstrate that nanoscale structural manipulation of the organic component can significantly change macroscale physical properties.

UV-induced cationic photopolymerization of epoxy monomers is a well-known process and of great interest as a result of its high number of industrial applications. The UV-polymerizable formulations are solvent free, the production rates are high, and the energy required is much less compared to thermal curing. Besides, cationic photopolymerization of epoxy monomers have some distinct advantages, such as lack of inhibition of oxygen, low shrinkage, and good mechanical properties of the UV-cured materials. The initiation of cationic UV-curing polymerization is a multistep process involving first, the photoexcitation of diaryliodonium or triarysulfonium salts, and then the decay of the resulting excited single state with both, heterelytic and homolytic cleavages: cations and aryl-cations generated are very reactive with monomers to give the formation of a Bronsted acid, which is the actual initiator of cationic polymerization.[24] Initiation of polymerization takes place by protonation of the monomer, followed by the addition of further monomer molecules, thus resulting in chain growth reaction.[25,26]

In a previous study, we prepared a novel epoxy nanocomposite possessing a low value of D_k by introducing a fluorine-containing POSS structure into the photopolymerization system.[27] In this present study, we first synthesized the OG monomer and then hybridized it with DGEBA and UVI 6976 to prepare a UV-cured epoxy resin. We expected the OG monomer units to be incorporated into the backbone of the epoxy resin upon UV curing. Herein, we discuss the morphologies and thermal properties of the prepared nanocomposites.

EXPERIMENTAL

Materials

The octakis(dimethylsilyloxy)silsesquioxane $(HMe_2SiOSiO_{1.5})_8$ ($Q_8M_8^H$) and platinum 1,3-divinyl-1,1,3,3-tetramethyldisiloxane [Pt(dvs)] were purchased from Aldrich Chemical Co. (USA). The allyl glycidyl ether (AGE) was purchased from Acros (Belgium). The DGEBA (EEW = 188 g/eq.) was purchased from Nan Ya Plastic Co. (Taiwan). The triarylsulfonium hexafluoroantimonate (UVI 6976, photoinitiator) was purchased from Dow Chemical Co. (USA). The chemical structures of these compounds are provided in Scheme 1.

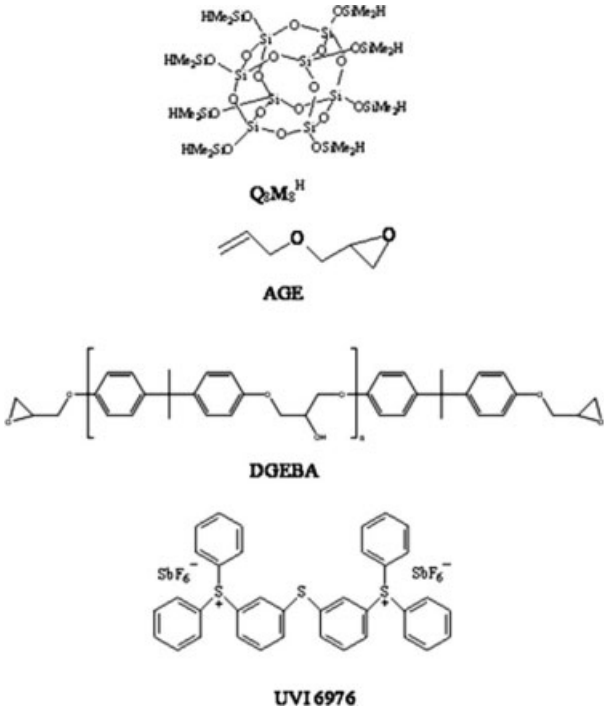

Scheme 1. Chemical structures of $Q_8M_8^H$, AGE, DGEBA, and UVI 6976.

Octakis(dimethylsiloxypropylglycidyl ether)silsesquioxane (OG)[19]

A solution of $Q_8M_8^H$ (0.50 g, 0.49 mmol) in toluene (5 mL) was stirred magnetically for 5 min in a 25-mL Schlenk flask. AGE (0.46 mL, 3.92 mmol) was then added, followed by 2.0 mM Pt(dvs) (10 drops). The reaction mixture was stirred at 80 °C for 8 h, cooled, and then dry activated charcoal was added. After stirring for 10 min, the mixture was filtered through a 0.45-μm Teflon membrane into a vial and stored as a clear solution having a concentration of 10 wt %. The solvent was evaporated and an opaque viscous liquid was obtained (0.86 g, 90%). The synthetic reaction is presented in Scheme 2. The molecular weight of the OG POSS was 1818.9 g/mol.

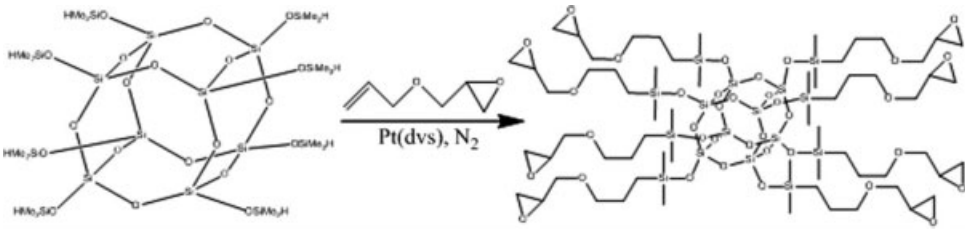

Scheme 2. Synthesis of OG.

Epoxy/POSS Nanocomposites

Table 1 lists the codes and compositions used in this study. The compositions are based on weight ratio. The photoinitiator (UVI 6976) used in all the composition was 5 phr. In a typical process, photopolymerization was performed by placing the sample mixture onto a glass plate at a thickness of 300 μm. A 180-W medium-pressure arc lamp ($\lambda_{max} = 366$ nm) was then used to irradiate the sample at a distance of 10 cm for 60 min at room temperature. The UV-cured sample was then heated (postcured) at 160 °C for 2 h. The structure of the fully-cured epoxy/OG nanocomposites is shown in Scheme 3.

Characterization

Proton Nuclear Magnetic Resonance (^{1}H NMR) Spectroscopy

^{1}H NMR spectra were recorded from $CDCl_3$ solutions using a Bruker AMX-500 FT NMR spectrometer operated at 500 MHz.

Fourier Transform Infrared (FTIR) Spectroscopy

FTIR spectra were recorded on a Perkin–Elmer Spectra One infrared spectrometer; 32 scans were collected with a spectral resolution of 1 cm^{-1}. FTIR spectra of the epoxy hybrid films were recorded from samples prepared using conventional NaCl disk methods. The hybrid was cast onto a NaCl disk, which was dried under conditions similar to those used for the bulk preparation. The films obtained in this way were sufficiently thin to obey the Beer-Lambert law.

Raman Spectroscopy

Raman spectra of the epoxy/POSS films were recorded using a Renishaw 2000 Raman spectrometer equipped with a He-Ne laser (1 mW) to irradiate the sample at a wavelength of 785 nm and a charge-coupled device (CCD) detector operating at a resolution of 1 cm^{-1}.

Differential Scanning Calorimetry (DSC)

DSC measurements were performed under a nitrogen atmosphere using a Perkin–Elmer DSC-7 differential scanning calorimeter. Each sample (~5 mg) was heated from 30 to 250 °C at a heating rate of 10 °C/min. The T_g temperature was taken as the midpoint of the capacity change.

Thermogravimetric Analysis (TGA)

A Perkin–Elmer thermogravimetric analyzer (TGA-7) was used to investigate the thermal stability of the nanocomposites. The samples (~5 mg) were heated under a nitrogen atmosphere from ambient temperature to 800 °C at a heating rate of 10 °C/min. The thermal degradation temperature was taken as the onset temperature at which a weight loss of 5 wt % occurred.

Dynamic Mechanical Analysis (DMA)

DMA measurements were performed using a TA Instruments DMA Q800 (DuPont) apparatus operated in a tensile film mode over a temperature range from 30 to 250 °C. Data acquisition and analysis of the storage modulus (E'), loss modulus (E''), and loss tangent (tan δ) were recorded automatically by the system. The heating rate and frequency were fixed at 3 °C/min and

Table 1. Codes and Compositions Used in this Study

Code	Composition
DGEBA/OG0	DGEBA:UVI 6976:OG = 100:5:0 (phr)
DGEBA/OG2	DGEBA:UVI 6976:OG = 100:5:2 (phr)
DGEBA/OG5	DGEBA:UVI 6976:OG = 100:5:5 (phr)
DGEBA/OG10	DGEBA:UVI 6976:OG = 100:5:10 (phr)
DGEBA/OG20	DGEBA:UVI 6976:OG = 100:5:20 (phr)

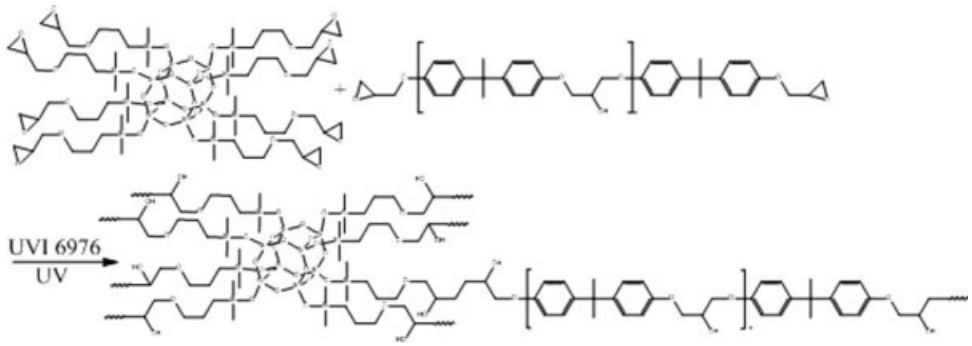

Scheme 3. Formation of epoxy/OG nanocomposites.

1 Hz, respectively. The sample's dimensions were $4 \times 0.4 \times 0.03$ cm.

Scanning Electron Microscopy (SEM)

Samples of the epoxy/POSS nanocomposites were fractured cryogenically with liquid N_2. The cryogenically fractured surfaces of the specimens were coated with thin layers of Pt and then their morphologies were examined under a Hitachi S-4700I scanning electron microscope.

RESULTS AND DISCUSSION

Characterization of OG

Figure 1 presents the ^{1}H NMR spectra of $Q_8M_8{}^H$ and OG. The chemical shifts of the signals for the CH_3 and SiH groups of $Q_8M_8{}^H$ appear at 0.11 and 4.71 ppm, respectively.[28] The chemical shifts of the signals for the protons of the $SiCH_2CH_2$ groups of OG appear at 0.57 and 1.60 ppm; no signal appears at 4.71 ppm, revealing that all of the SiH groups had reacted. Figure 2 displays the ^{13}C NMR spectrum of OG; the signal for the carbon atoms of the CH_3 groups appears at -0.5 ppm and those for the epoxy groups appear at 50.6 and 44.0 ppm. Figure 3 provides the FTIR spectra of

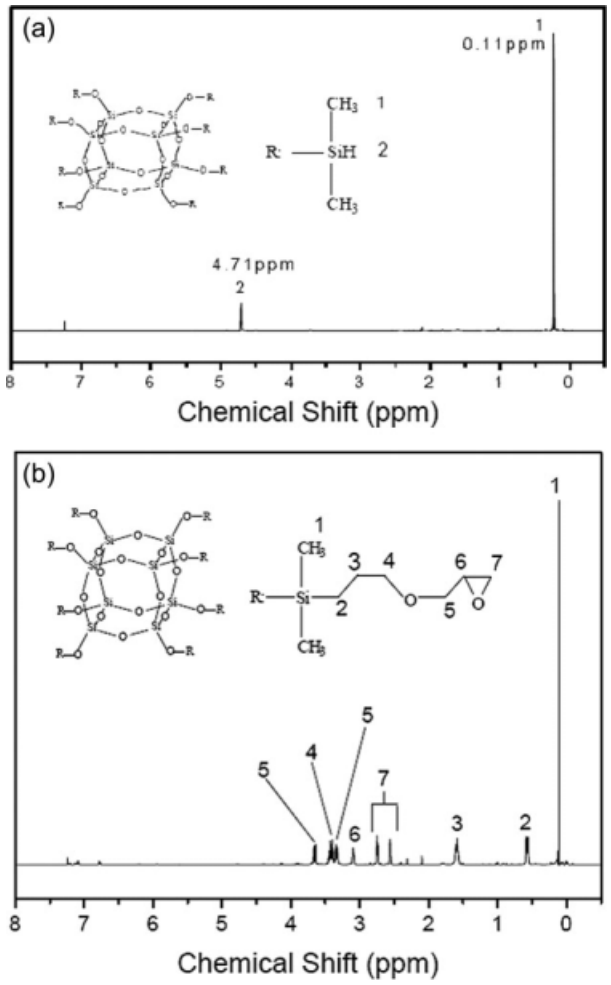

Figure 1. ^{1}H NMR spectra of (a) $Q_8M_8{}^H$ and (b) OG.

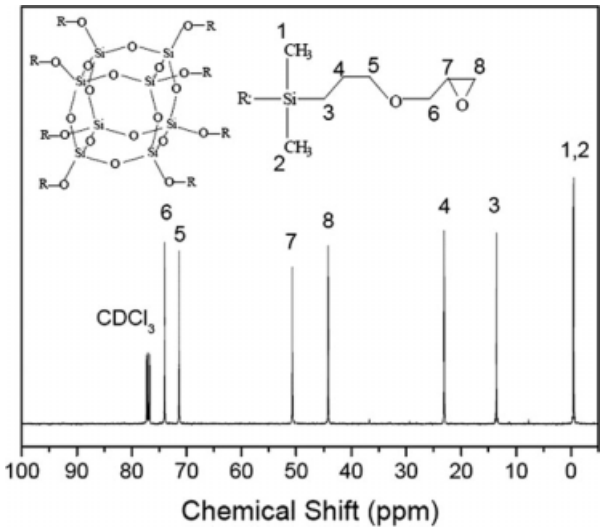

Figure 2. ^{13}C NMR spectrum of OG.

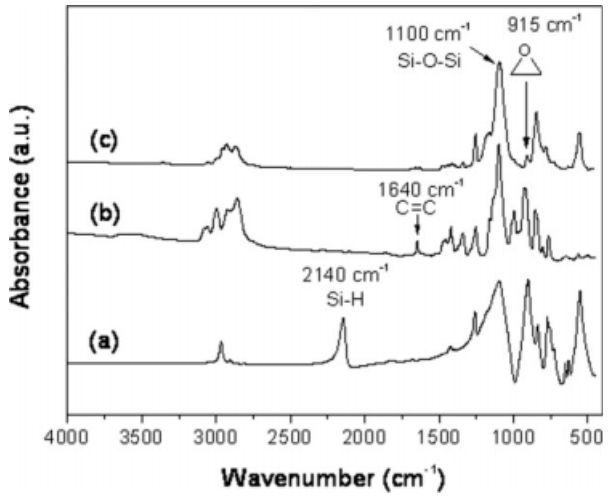

Figure 3. FTIR spectra of (a) $Q_8M_8^H$, (b) AGE, and (c) OG.

$Q_8M_8^H$, AGE, and OG. In the FTIR spectrum of $Q_8M_8^H$, we observe a sharp, strong, and symmetric peak at 1100 cm^{-1} corresponding to stretching of the Si—O—Si units of the silsequioxane cage and a Si—H stretching peak at 2140 cm^{-1}.[19,29,30] The presence of the signal at 1100 cm^{-1} reveals that the cube structure survived during processing; if it had degraded, we would observe a shift to the asymmetric broad peaks that are typical of silica.[31,32] In the FTIR spectrum of AGE, we observe a small CH_2=CH stretching peak at 1640 cm^{-1} and an epoxy ring asymmetric stretching peak at 915 cm^{-1}. The signals of both the Si—H and CH_2=CH units are absent from the FTIR spectrum of OG, implying that hydrosilylation had occurred successfully to form the POSS

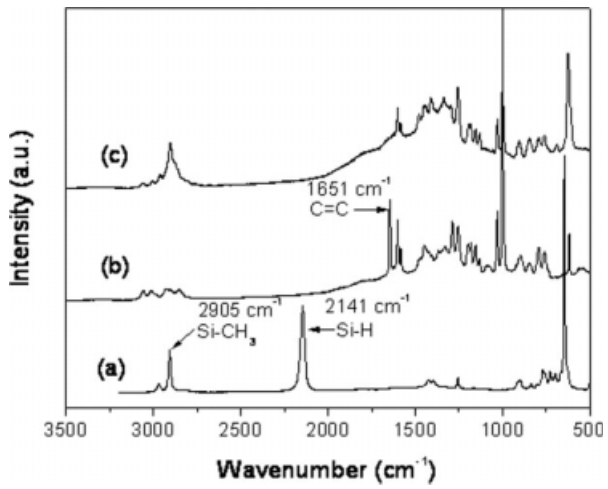

Figure 4. Raman spectra of (a) $Q_8M_8^H$, (b) AGE, and (c) OG.

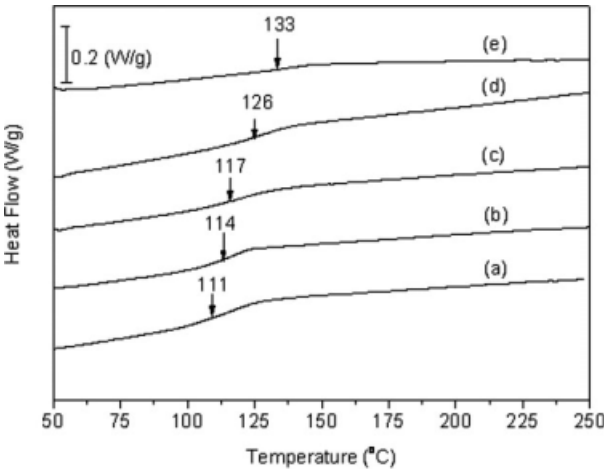

Figure 5. DSC thermograms of epoxy/POSS nanocomposites containing OG contents of (a) 0, (b) 2, (c) 5, (d) 10, and (e) 20 phr.

derivative presenting epoxy rings. Figure 4 presents the Raman spectra of $Q_8M_8^H$, AGE, and OG. We assign the peaks at 2905 and 2140 cm^{-1} to the Si—CH_3 and Si—H stretching modes, respectively, of $Q_8M_8^H$ and the signal at 1651 cm^{-1} to the C=C backbone stretching of AGE. As expected, the signals at 2140 and 1651 cm^{-1} were absent from the Raman spectrum of OG. Taken together, the FTIR, Raman, and NMR spectra confirmed that $Q_8M_8^H$ did indeed react with AGE through hydrosilylation to form OG.

Glass Transition Temperature

We used DSC and DMA to determine the T_g temperatures of the epoxy/POSS nanocomposites. Figure 5 displays the DSC thermograms obtained from epoxy/POSS nanocomposites containing various contents of OG; Table 2 summarizes the results. A single value of T_g existed for each of the nanocomposites. The T_g temperatures of the OG-

Table 2. Glass Transition Temperatures and Heat Capacities of the Epoxy and Epoxy/POSS Nanocomposites

	DSC		DMA	
Code	T_g (°C)	DCp (J/g °C)	T_g (°C)	tan δ
DGEBA/OG0	111.3	0.321	125.2	0.70
DGEBA/OG2	114.5	0.304	130.5	0.67
DGEBA/OG5	117.4	0.255	132.3	0.62
DGEBA/OG10	126.2	0.202	136.4	0.52
DGEBA/OG20	133.3	0.134	142.8	0.40

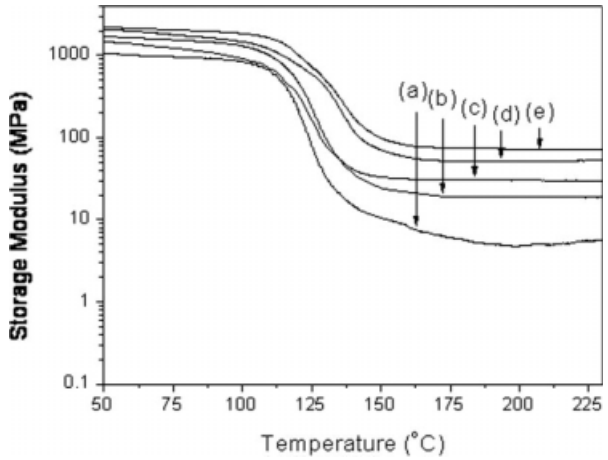

Figure 6. Storage moduli of epoxy/POSS nanocomposites containing OG contents of (a) 0, (b) 2, (c) 5, (d) 10, and (e) 20 phr.

containing epoxy nanocomposites were higher than that of the plain epoxy; in addition, the value of T_g increased upon increasing the OG content.

Viscoelastic Properties of the Epoxy/POSS Nanocomposites

Figure 6 displays the storage modulus (E') of the pure epoxy and the epoxy/POSS nanocomposites recorded over the temperature range from 50 to 225 °C. For the epoxy resin, the modulus decreased continuously upon increasing the temperature above its T_g temperature. The values of E' values of the hybrids were all higher than that of the pure epoxy. In addition, the values of E' of the nanocomposites containing greater OG contents remains more of less constant at higher temperatures. In the rubber state, we found that the epoxy/POSS nanocomposites possessed higher values of T_g when they contained higher OG contents. We attribute this behavior to a significant nano-reinforcement effect of the POSS cages on the epoxy networks. Because the nanometer-scale POSS cages restrict the motion of the macromolecular chains, higher temperatures are required to provide the requisite thermal energy for the T_g to occur in the hybrid materials.[14] Furthermore, because the OG monomers reacted with the epoxy units, their presence increased the crosslink density relative to that in the epoxy-only matrix. The plot of tan δ versus temperature for a cured epoxy provides the major relaxation transition, corresponding to the value of T_g of the cured epoxy resin. Figure 7 provides the tan δ plot of the DMA thermogram data of the cured epoxy and epoxy/POSS nanocomposites containing various amounts of OG. The maximum tan δ peak of the UV-cured epoxy resin occurred at a temperature of 125.2 °C. The T_g temperatures increased upon increasing the OG content (Table 2); for example, that of the epoxy/POSS nanocomposite featuring an OG content of 20 phr was 142.8 °C, significantly higher than that of the neat epoxy. Again, this behavior reflects the significant nano-reinforcement effect of the POSS cages and the increased crosslink density that existed after the reaction between epoxy and OG; i.e., the incorporation of POSS cages into the epoxy network hinders the movement of the polymer chains and, thereby, results in higher values of T_g. In addition, Figure 7 also reveals a slight depression in the peak intensity upon increasing the OG content. Because the damping properties are provided by the ratio of the viscous and elastic components, we surmise that a reduced peak height is associated with a lower segmental mobility and fewer relaxation species and, therefore, it is indicative of stronger bonding for the epoxy/POSS nanocomposites. Moreover, the width of the peak in the tan δ plot reflects the degree of structural homogeneity in a crosslinked network; for our system, the peak width at half height increased upon increasing the OG content—a result of decreasing network homogeneity.[19,33] Presumably, the broadening of the T_g region resulted from the incorporation of the relatively bulky (nanometer-sized) POSS cages, which restricted the segmental

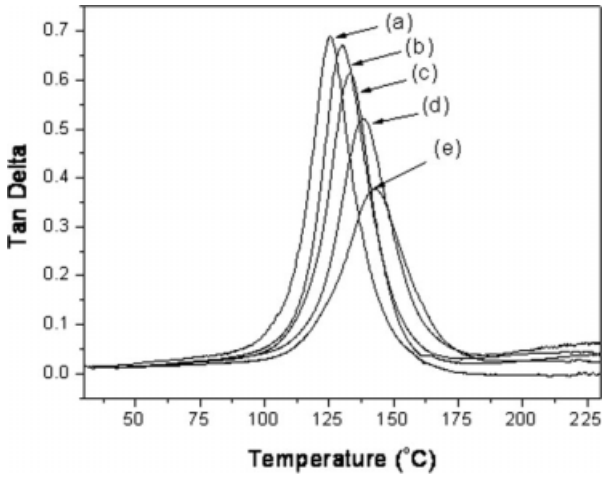

Figure 7. Plots of tan δ of the epoxy/POSS nanocomposites containing OG contents of (a) 0, (b) 2, (c) 5, (d) 10, and (e) 20 phr.

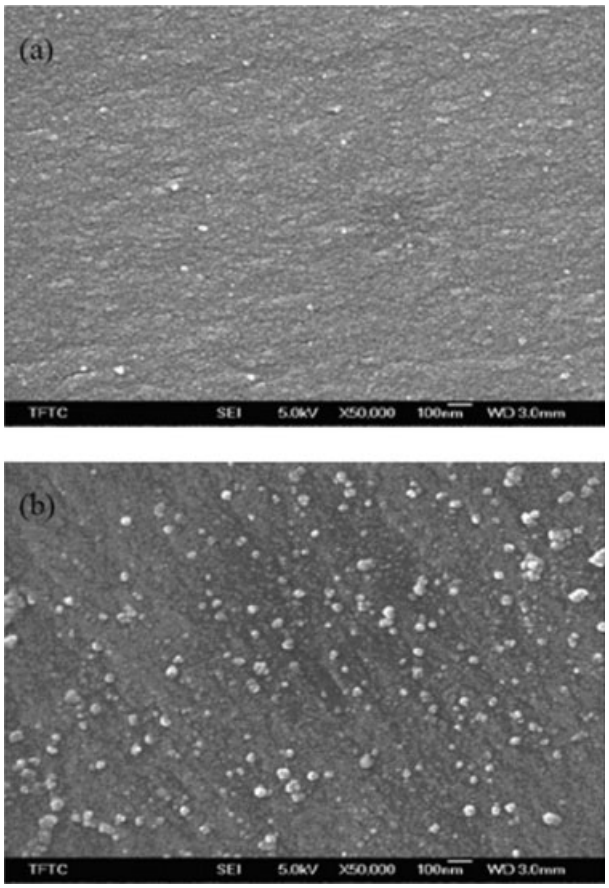

Figure 8. SEM micrographs of epoxy/POSS nanocomposites containing OG contents of (a) 2 and (b) 10 phr.

motion of the polymer chains and network junctions. Therefore, higher temperatures were required to reach structural equilibrium.[34]

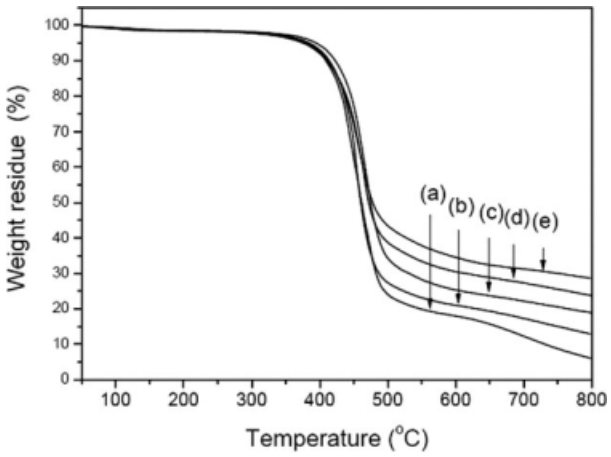

Figure 9. TGA thermograms of epoxy/POSS nanocomposites containing OG contents of (a) 0, (b) 2, (c) 5, (d) 10, and (e) 20 phr.

Table 3. Thermal Properties of the Epoxy and Epoxy/POSS Nanocomposites

Code	T_5 (°C, 5 wt % loss)	Char Yield (wt %) at 800 °C
DGEBA/OG0	380.4	6.05
DGEBA/OG2	384.5	12.92
DGEBA/OG5	394.3	18.91
DGEBA/OG10	380.8	23.74
DGEBA/OG20	375.3	28.65

Morphology of the Epoxy/POSS Nanocomposites

Figure 8 presents SEM micrographs of the fractured surfaces of epoxy/POSS nanocomposite specimens created by freezing in liquid N_2. The particle size of the OG units in the epoxy/POSS (2 phr OG) nanocomposite was ~10 to 30 nm; it increased upon increasing the OG content in the nanocomposites. For the epoxy/POSS (10 phr OG) nanocomposite, the particle size of the OG units was ~20 to 60 nm because of the immiscibility of OG and the cured epoxy.

Thermal Stability of the Epoxy/POSS Nanocomposites

Figure 9 and Table 3 provide TGA thermograms and data, respectively, recorded under a N_2 atmosphere for the epoxy resins containing various OG contents. The 5 wt % weight loss temperature (T_5) increased upon increasing the OG content up to 5 wt %, but decreased thereafter, presumably because of excess aggregation at higher OG contents. In contrast, the char yields of the epoxy/POSS nanocomposites increased upon increasing the OG content. This result is not surprising because when POSS structures are degraded thermally they typically form SiO_2, which results in higher char yields.[30]

CONCLUSIONS

We have prepared epoxy/POSS nanocomposites through photopolymerization of OG and the diglycidyl ether of bisphenol A, and characterized them using NMR, Raman, and FTIR spectroscopies. DSC analysis indicated that a single T_g occurred for each nanocomposite, with the value of T_g increasing upon increasing the content of OG. DMA revealed that the nanocomposites exhibited enhanced storage moduli in the rubbery state, which we ascribe to (i) the nano-

reinforcement effect of the POSS cages and (ii) the increased degree of crosslinking that resulted from the reactions between the epoxy and OG. The addition of OG to the epoxy network increased the crosslinking density substantially and improved the thermal properties, as evidenced from TGA measurements.

The authors thank the National Science Council (Taiwan, Republic of China) for supporting this research financially under contract no. NSC-94-2216-E-238-003.

REFERENCES AND NOTES

1. Haddad, T. S.; Lichtenhan, J. D. Macromolecules 1996, 29, 7302–7304.
2. Xu, H.; Kuo, S. W.; Lee, J. S.; Chang, F. C. Macromolecules 2002, 35, 8788–8793.
3. Ciolacu, F. C. L.; Choudhury, N. R.; Dutta, N.; Kosior, E. Macromolecules 2007, 40, 265–272.
4. Misra, R.; Fu, B. X.; Morgan, S. E. J Polym Sci Part B: Polym Phys 2007, 45, 2441–2455.
5. Li, H.; Zheng, S. Macromol Rapid Commun 2005, 26, 196–200.
6. Lu, T. L.; Liang, G. Z.; Guo, Z. J Appl Polym Sci 2006, 101, 3652–3658.
7. Lichtenhan, K. D.; Otonari, Y. A.; Carr, M. J. Macromolecules 1995, 28, 8435–8437.
8. Li, C.; Wilkes, G. Chem Mater 2001, 13, 3663–3668.
9. Zeng, Q. H.; Wang, D. Z.; Yu, A. B.; Lu, G. Q. Nanotechnology 2002, 13, 549–553.
10. Chen, C.; Curliss, D. Nanotechnology 2003, 14, 643–648.
11. Liu, Y. L.; Chang, G. P. J Polym Sci Part A: Polym Chem 2006, 44, 1869–1876.
12. Chen, W. Y.; Wang, Y. Z.; Kuo, S. W.; Huang, C. F.; Tung, P. H.; Chang, F. C. Polymer 2004, 45, 6897–6908.
13. Ni, Y.; Zheng, S.; Nie, K. M. Polymer 2004, 45, 5557–5568.
14. Lee, A.; Lichtenhan, J. D. Macromolecules 1998, 31, 4970–4974.
15. Liu, Y. L.; Chang, G. P.; Hsu, K. Y.; Chang, F. C. J Polym Sci Part A: Polym Chem 2006, 44, 3825–3835.
16. Maria, J. A.; Luis, B.; Diana, P. F.; Roberto, J. J. W. Macromolecules 2003, 36, 3128–3135.
17. Li, G. Z.; Wang, L.; Toghiani, H.; Daulton, T. L.; Pittman, C. U., Jr. Polymer 2002, 43, 4167–4176.
18. Ramirez, C.; Abad, M. J.; Barral, L.; Cano, J.; Diez, F. J.; Lopez, J.; Montes, R.; Polo, J. J Therm Anal Calor 2003, 72, 421–429.
19. Choi, J.; Harcup, J.; Yee, A. F.; Zhu, Q.; Laine, R. M. J Am Chem Soc 2001, 123, 11420–11430.
20. Sellinger, A.; Laine, R. M. Chem Mater 1996, 9, 1592–1593.
21. Choi, J.; Yee, A. F.; Laine, R. M. Macromolecules 2003, 36, 5666–5682.
22. Choi, J.; Kim, S. G.; Laine, R. M. Macromolecules 2004, 37, 99–109.
23. Choi, J.; Yee, A. F.; Laine, R. M. Macromolecules 2004, 37, 3267–3276.
24. Dektar, J. L.; Hacker, N. P. J Org Chem 1990, 55, 639–647.
25. Crivello, J. V. J Polym Sci Part A: Polym Chem 1999, 37, 4241–4254.
26. Sangermano, M.; Bongiovanni, R.; Priola, A.; Pospiech, D. J Polym Sci Part A: Polym Chem 2005, 43, 4144–4150.
27. Wang, Y. Z.; Chen, W. Y.; Yang, C. C.; Lin, C. L.; Chang, F. C. J Polym Sci Part B: Polym Phys 2007, 45, 502–510.
28. Yang, C. C.; Chang, F. C.; Wang, Y. Z.; Chan, C. M.; Lin, C. L.; Chen, W. Y. J Polym Res 2007, 14, 431–439.
29. Marcolli, C.; Calzaferri, G. Appl Organomet Chem 1999, 13, 213–226.
30. Wallace, W. E.; Guttman, C. U.; Antoucci, J. M. Polymer 2000, 41, 2219–2226.
31. Silverstein, R. M.; Webster, F. X. Spectrometric Identification of Organic Compounds; Wiley: New York, 1996.
32. Chen, Y.; Iroh, J. O. Chem Mater 1999, 11, 1218–1222.
33. Huang, J. M.; Kuo, S. W.; Lee, Y. J.; Chang, F. C. J Polym Sci Part B: Polym Phys 2007, 45, 644–653.
34. Lee, A.; Lichtenhan, J. D.; Reinerth, W. A. Polym Mater Sci Eng 2000, 82, 235–236.